UNIVERSITY OF BIRMINGHAM
University of Birmingham Research at Birmingham

Passive multistatic SAR with GNSS transmitters and using joint bi/multi-static CLEAN technique

Santi, F.; Bucciarelli, M.; Pastina, D.; Antoniou, Michail; Cherniakov, Mikhail

DOI:
10.1109/RADAR.2016.7485109

License:
None: All rights reserved

Document Version
Peer reviewed version

Citation for published version (Harvard):
Santi, F, Bucciarelli, M, Pastina, D, Antoniou, M & Cherniakov, M 2016, Passive multistatic SAR with GNSS transmitters and using joint bi/multi-static CLEAN technique. in *2016 IEEE Radar Conference, RadarConf 2016.*, 7485109, Institute of Electrical and Electronics Engineers (IEEE), 2016 IEEE Radar Conference, RadarConf 2016, Philadelphia, United States, 2/05/16. https://doi.org/10.1109/RADAR.2016.7485109

Link to publication on Research at Birmingham portal

Publisher Rights Statement:
(c) 2016 IEEE. Personal use of this material is permitted. Permission from IEEE must be obtained for all other users, including reprinting/ republishing this material for advertising or promotional purposes, creating new collective works for resale or redistribution to servers or lists, or reuse of any copyrighted components of this work in other works.

Checked 29/7/2016

General rights
Unless a licence is specified above, all rights (including copyright and moral rights) in this document are retained by the authors and/or the copyright holders. The express permission of the copyright holder must be obtained for any use of this material other than for purposes permitted by law.

•Users may freely distribute the URL that is used to identify this publication.
•Users may download and/or print one copy of the publication from the University of Birmingham research portal for the purpose of private study or non-commercial research.
•User may use extracts from the document in line with the concept of 'fair dealing' under the Copyright, Designs and Patents Act 1988 (?)
•Users may not further distribute the material nor use it for the purposes of commercial gain.

Where a licence is displayed above, please note the terms and conditions of the licence govern your use of this document.

When citing, please reference the published version.

Take down policy
While the University of Birmingham exercises care and attention in making items available there are rare occasions when an item has been uploaded in error or has been deemed to be commercially or otherwise sensitive.

If you believe that this is the case for this document, please contact UBIRA@lists.bham.ac.uk providing details and we will remove access to the work immediately and investigate.

Download date: 26. Apr. 2024

Passive Multistatic SAR with GNSS Transmitters and Using Joint Bi/Multi-static CLEAN Technique

F. Santi[a], M. Bucciarelli[a], D. Pastina[a], M. Antoniou[b], M. Cherniakov[b]

[a]Department of Information Engineering, Electronics and Telecommunications
University of Rome "La Sapienza", Rome, Italy
santi@diet.uniroma1.it, mbucciarelli@infocom.uniroma1.it, debora@infocom.uniroma1.it

[b]Microwave Integrated Systems Laboratory
University of Birmingham, Birmingham, United Kingdom
m.antoniou@bham.ac.uk, m.cherniakov@bham.ac.uk

***Abstract*—This paper explores the capability of GNSS as opportunity transmitters for passive multistatic SAR. The large number of navigation satellites illuminating the same area from multiple view angles enables a single ground-based stationary receiver to combine the individual bistatic images thus achieving multistatic imagery capability with improved spatial resolution. Nevertheless, such a technique introduces artifacts corrupting the quality of the image information space. In this paper, a joint bi/multi-static CLEAN algorithm is exploited in order to correctly recovering the information of the scene. An experimental study is therefore presented, demonstrating the potential of this technology to extract detailed information of an area for persistent monitoring purposes.**

Keywords—multistatic SAR, passive SAR, GNSS-based SAR, resolution improvement, CLEAN

I. INTRODUCTION

Over the recent years, Bistatic Synthetic Aperture Radar (BSAR) based on Global Navigation Satellite Systems (GNSS) has been the focus of an increased research activity [1]. A number of reasons supports the choice of navigation satellites as opportunity transmitters for SAR applications. First, as GNSS-based SAR is a passive system, it allows low-cost, license-free and covert operations. Furthermore, GNSSs are satellite constellations designed for continuous and global coverage, therefore enabling persistent area monitoring. On the other hand, GNSS are not designed for remote sensing purposes and therefore lack the power budget and resolution capabilities of dedicated SARs. Nevertheless, by long dwell times on target, in the order of several minutes for a fixed receiver, suitable Signal-to-Noise-Ratio (SNR) can be achieved, along with an azimuth resolution of few meters (3-4m for 4-5 mins dwell). The fundamental bottleneck lies in the range resolution, which is defined by the ranging signal bandwidth. As example, GLONASS P-code, having a chip rate of 5.11 MHz, offers a maximum range resolution of 30m. Moreover, the bistatic acquisition geometry can drastically worsen the spatial resolution of the system [2]. This limitation restricts the field of application for this technology and for this reason some efforts have been made to improve the spatial resolution of the system exploiting a single transmitter [3].

A widely employed approach to improve the resolution capability of a radar system is to consider multiple, spatially dispersed transmitting and/or receiving stations. By combining coherently or incoherently the signals received from each receiving channel, an enhanced ambiguity function of the system can be obtained [4]. From this point of view, GNSS are an ideal choice: a single constellation guarantees that 6-8 satellites are simultaneously in visibility over the horizon, and this number can be increased up to 32 when all the GNSS are fully operational. All of these signals can be received and processed separately or jointly by a stationary ground-based receiver, essentially forming a passive multistatic radar system [5-8]. In our latest research [6] it was shown that the incoherent addition of the individual bistatic ambiguity functions obtained by multiple, spatially separated GNSS transmitters can yield multistatic imagery that may essentially enhance spatial resolution with respect to the individual images. The improved spatial resolution is able to reveal more details of the observed area; nevertheless, such technique introduces artifacts at the image level that should be corrected [7].

New advances on this research topic are presented in this paper. The improved spatial resolution of the multistatic SAR (MSAR) image provides the capability to identify with enhanced accuracy the scattering centers composing the scene. In order to localize the scattering centers, ad-hoc CLEAN algorithms able to deal with both bistatic and multistatic GNSS-based SAR images have been preliminary developed and assessed in [9]. Here, by employing an improved variant of the multistatic CLEAN algorithm, the point features of the MSAR image are extracted. The effectiveness of the proposed technique to correctly recovering the information contained in the MSAR image is preliminarily tested against experimental point targets. Then, the technique has been applied against experimental images, showing the potential of the multistatic approach to provide a deeper degree of details of the observed area with respect to the case where the point features are extracted from the bistatic image.

The paper is organized as follows: Section II introduces the GNSS-based MSAR concept; the proposed multistatic CLEAN algorithm is presented in Section III and in Section IV the results obtained against experimental images are shown; conclusions are drawn in Section V.

II. GNSS-BASED MULTISTATIC SAR

The operative condition is given by a ground-based stationary receiver covering with its antenna footprint the area of interest recording the signal reflections from *N* GNSS satellites; a second antenna collects the direct signals for the synchronization procedure. As GNSSs operate on frequency or coding division basis, the receiver can separate the signal coming from different satellites; then, by using proper focusing technique [10], *N* BSAR images of the area are obtained.

The coarse spatial resolution of the system allows considering the scene as composed by a set of isolated and point-like targets. Therefore, the *i*th ($i = 1, \dots, N$) BSAR image I_i can be considered as the coherent superposition of *K* Point Spread Functions (PSFs) centered in the *k*th scatterer position and scaled for a complex coefficient accounting for its reflectivity as viewed in the *i*th perspective:

$$I_i = \sum_{k=1}^{K} \xi_{ik} \chi_i(e - e_k, n - n_k) \qquad (1)$$

In (1), ξ is the complex reflectivity of the scatterer and χ is the space variant PSF of the system for the scatterer point located in (e_k, n_k) in the East-North-Up reference system centered in the receiver position (analytical details for the PSF evaluation can be found in [11]).

An ideal scattering point gives rise to a spot in the image that can be well approximated as an ellipse, whose area is in the order of 100 m^2, because of the limited transmitted bandwidth and the bistatic acquisition geometry. As example, Fig. 1a and b show the bistatic PSF resulting from two differently located GLONASS transmitters for 300 s dwell; wide resolution cell areas have been obtained for both the cases, with area (at the -3 dB cut) equal to 98 m^2 (a) and 80 m^2 (b).

By looking at the bistatic images responses, one can observe that from different satellite transmissions differently oriented PSFs have been obtained. The orientation of the individual PSF depends on the particular bistatic topology and therefore, when *N* different satellites are considered, *N* different orientations of the bistatic resolution cell can be obtained. This suggests the possibility to perform an incoherent integration of the individual images, in order to achieve a multistatic image that may be drastically improved in terms of spatial resolution [6]. The MSAR image I_M is therefore obtained as

$$I_M = \frac{1}{N} \sum_{i=1}^{N} |I_i| \qquad (2)$$

which it is expected to be characterized by a finer resolution cell. As example, in Fig. 1c the resulting MSAR image obtained from the incoherent addition of the bistatic responses in Fig. 1a and b is shown, resulting in a resolution cell area of 17 m^2.

When we move from point target analysis to complex scenarios, some additional considerations are in order. First, different bistatic geometries result in target radar cross section variation. Therefore, the multistatic response S_M of the system has to take into account different scatterer's amplitude $A_{ik} = |\xi_{ik}|$ in the different BSAR images:

$$S_{Mk} = \frac{1}{N} \sum_{i=1}^{N} |S_{ik}| = \frac{1}{N} \sum_{i=1}^{N} A_{ik} |\chi_i(e - e_k, n - n_k)| \qquad (3)$$

where $S_{ik} = \xi_{ik} \chi_i(e - e_k, n - n_k)$ is the bistatic response pertaining to the *i*th image. Nevertheless, it is easy to see that, despite the different amplitude coefficients, considerable improvement in spatial resolution may be obtained. As example, Fig. 1d shows the multistatic image obtained by adding the bistatic responses in Fig. 1a,b with amplitude coefficient $A_1 = 1$ and $A_2 = ½$; the resulting resolution cell area is equal to 18.5 m^2, still providing a significant improvement factor with respect to the individual images. Moreover, in a real scene the presence of multiple close scattering points is a usual situation. Depending on the relative scatterers positions and bistatic PSFs orientations, different situations can occur in the multistatic image. Fig. 1e shows the case of two scatterers aligned along the direction of the major axis of the image response in Fig. 1a: since such a direction represents the worst spatial resolution direction in the bistatic image [6], the scatterers are hard to be identified as separated. However, thanks to the intersections with the elliptical spots concerning the image response in Fig. 1b, in the MSAR image two distinct bright spots can be easily recognized. A different situation is depicted in Fig. 1f, where four spots can be observed: two of them result from the intersections of the bistatic responses of the same point target, whereas the remainders are false target positions (ghosts) due to the intersections of resolution ellipses concerning different targets.

It is worth to notice that same position of scattering centers in different images has been assumed. Fulfilling such a hypothesis requires a not excessive angular separation among the transmitters, since different perspectives result in decorrelation of the radar signatures. However, in this regard it is worth to notice that the GNSS-based SAR images are characterized by large resolution cell areas; roughly speaking, this results in moderate fluctuations of the target position even for not negligible variation of the looking angle. Moreover, the incoherent processing to obtain the MSAR image further relaxes the restriction on the angular separation among the transmitters. Lastly, bistatic PSF orientation depends on a number of factors, and even for satellites with close illumination angles different orientations can be obtained [6].

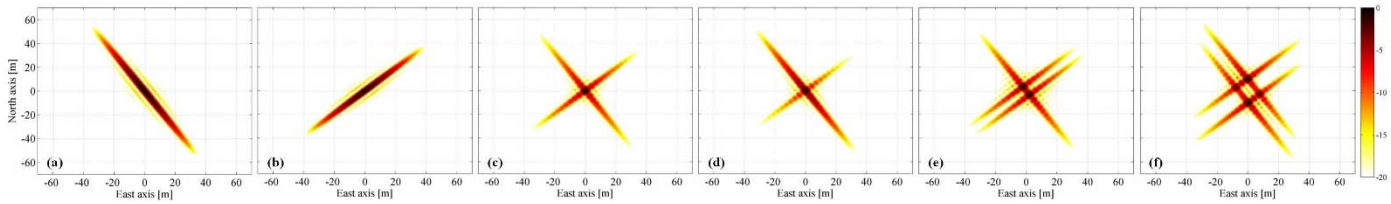

Figure 1. Examples of bi/multi-static images for point targets - bistatic images responses (a), (b); multistatic images of a single point target for A_1=A_2 (c) and A_2 = ½×A_1 (d); multistatic images of two close point targets located in #1: [-2.2 3.2] m, #2: [2.2 -3.2] m (e) and #1: [0 -10] m, #2: [0 10] m (f).

III. Feature Extraction Technique

In order to extract the point features from bistatic and multistatic GNSS-based SAR images, an ad-hoc CLEAN algorithm has been developed in [9]. Such an algorithm proved to be able to possess some capabilities in revealing scene information despite the poor spatial resolution of the system. Nevertheless, when applied against multistatic images, its performance is limited by the lack of the phase information. Indeed, the MSAR image is an incoherent sum of the single BSAR images, (2), and therefore, when the multistatic CLEAN is applied, the estimated image responses of each identified scatterers are subtracted incoherently from the image, corrupting the radiometric characteristic of the image and possibly masking weaker targets. Coherent variants of the CLEAN are able to greatly mitigate such a shortcoming, due to a more accurate subtraction of the scatterer point spread function from the image, deriving from the joint amplitude and phase information use. Since the phase information is retained in the bistatic (complex) images, in order to retrieve such information they have to be involved directly in the process. An enhanced version of the technique presented in [9] is here proposed, referred to as joint bi/multi-static CLEAN technique, which steps are detailed in the following subsection.

A. Joint bi/multi-static CLEAN for GNSS-based SAR images

The flowchart of the technique is depicted in Fig. 2. The proposed algorithm is an iterative procedure whose *k*th iteration consists in the following steps:

1) The brightest point of the MSAR image is selected.

2) The position and the N amplitudes of the corresponding scatterer in the N bistatic images are estimated as in [9] by minimizing a cost function defined as the energy of the difference of a patch I_M^{sel} of the MSAR image containing the scatterer and the model of the multistatic response

$$\min_{(A_{1k},\dots,A_{Nk},e_k,n_k)} \sum \left\{ \left| S_M(A_{1k},\dots,A_{Nk},e_k,n_k) - I_M^{sel} \right|^2 \right\} \quad (4)$$

Since the MSAR image provides better resolution than each of the bistatic images does, the estimated position $(\hat{e}_k, \hat{n}_k)$is assumed as the actual value, whereas the amplitudes are used as initial searching points in the following step. It is worth to notice that at this point the old version of the algorithm evaluated the multistatic response and subtracted it incoherently from the MSAR image. The steps highlighted by the blue dotted box in Fig. 2 therefore represent the novel part of the method with respect to [9].

3) The complex amplitudes are estimated as the ones jointly minimizing the cost functions of the bistatic/multistatic images; since the phase information is still preserved in the single BSAR, both modulus and phases of the single bistatic responses can be recovered

$$\min_{(\xi_{1k},\dots,\xi_{Nk})} \left\{ \begin{array}{l} \sum_{i=1}^{N} \left\{ \sum \left| S_i(\xi_{ik}; \hat{e}_k, \hat{n}_k) - I_i^{sel} \right|^2 \right\} + \\ + \sum \left\{ \left| S_M(|\xi_{1k}|,\dots,|\xi_{Nk}|; \hat{e}_k, \hat{n}_k) - I_M^{sel} \right|^2 \right\} \end{array} \right\} \quad (5)$$

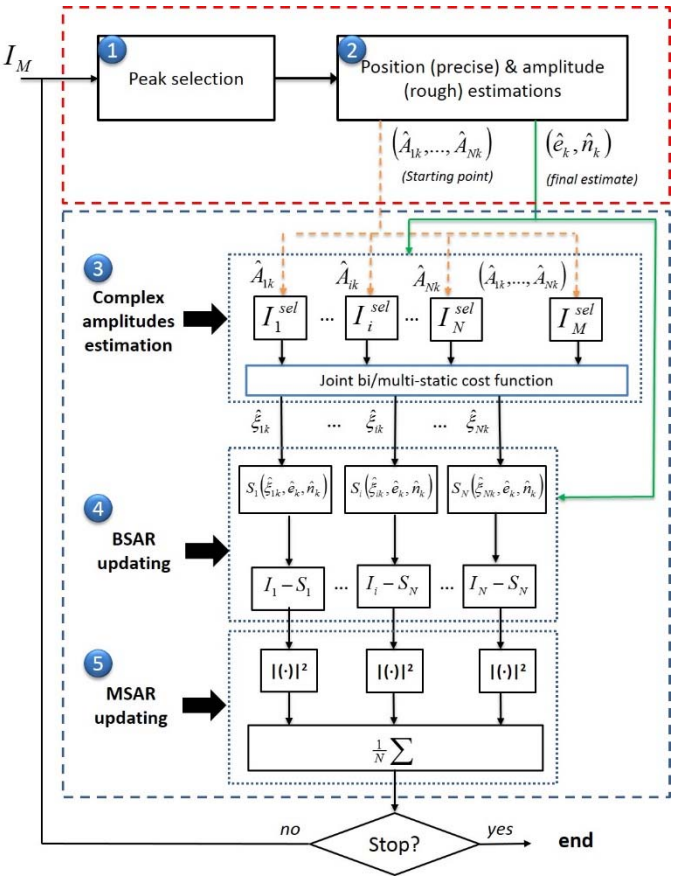

Figure 2. Flowchart of the joint bi/multi-static CLEAN technique.

4) The estimated bistatic responses are coherently subtracted from the corresponding BSARs:

$$I_i - S_i(\hat{\xi}_{ik}, \hat{e}_k, \hat{n}_k), \quad i = 1,\dots,N \quad (6)$$

5) The updated bistatic images are incoherently added to form the updated MSAR image as in (2).

Steps 1-5 are repeated until the energy of the image is below a proper threshold.

B. Performance analysis

Experimental PSFs [6] obtained from two GLONASS transmissions (hereinafter sat. A and sat. B) have been used to emulate bi/multi-static images of point targets, here employed to preliminarily assess the performance of the algorithm.

In a first case study, for both sat. A and sat. B, BSAR images composed by two scatterers have been emulated by coherently adding experimental PSFs with a phase difference selected according to a uniform distribution in [-π ,π) and a white Gaussian noise as disturbance resulting in peak SNR equal to 25 dB. The scatterers have been located at distance ΔR onto the major axis of the resolution ellipse concerning sat. A. Then, by a non-coherent combination, the MSAR image is obtained (an example is shown in Fig. 3a). 1000 independent trials have been carried out for every ΔR under test, and the probability of correct feature extraction $P_{c.e.}$ has been evaluated. A correct extraction is assumed if the following conditions are

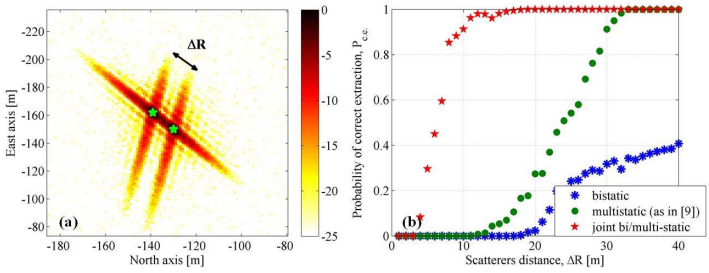

Figure 3. Close scatterers aligned onto the major axis of the bistatic resolution cell – a) example of MSAR image, b) probability of correct feature extraction.

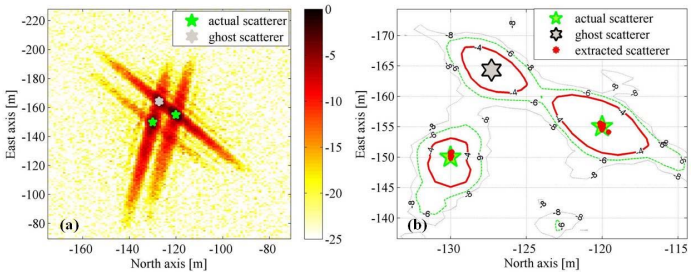

Figure 4. De-ghosting capability – a) MSAR image, b) isolevel curves with actual, ghost and extracted scatterers.

concurrently fulfilled: (i) both the scatterers are identified, (ii) the maximum error on scatterer positions is lower than a threshold δP and (iii) the maximum error on scatterer amplitudes is lower than a threshold δA. Fig. 2b shows the obtained results, comparing the performance of the joint bi/multi-static CLEAN in the bistatic (sat. A) and multistatic cases (bistatic case is obtained as the special cases of two coinciding images). As it is apparent, drastically enhanced capability of correctly recovering the scene information has been obtained in the multistatic scenario, being the bistatic case performance severely limited by the poor resolution in the direction over which the scatterers are aligned. Furthermore, a considerably great improvement of the performance has been obtained with respect to the previous version of the multistatic algorithm [9], therefore allowing for a successful identification of closer scatterers.

In a second analysis, we aim at proving the inherent de-ghosting capability of the algorithm. In this case, scatterers positions are $\mathbf{P}_1$=(-130m, -150m) and $\mathbf{P}_2$=(-120m, -155m), with amplitudes A_1=1, A_2=0.8 (BSAR sat. A) and A_1=0.4, A_2=1 (BSAR sat. B). The resulting MSAR image is shown in Fig. 4a and one can observe that in these particular conditions a ghost target appears. Twenty independent trials have been carried out with a noise floor as in the previous analysis. Extracted scatterers positions are showed in Fig. 4b (red '*' markers), superimposed to the contour plots of the MSAR image. One can observe that the ghost target has never been identified as a real multistatic return, whereas real scatterers have been extracted with an accuracy in the order of 1 m. This is a consequence of the iterative procedure of the CLEAN: when the first multistatic return is subtracted from the image, the intersections originating the ghost disappear.

IV. Experimental Results

Experiments were conducted on the roof of the School of Electronic, Electrical and Computer Engineering of the University of Birmingham (UK). The receiver, shown in Fig. 5, uses a low-gain antenna to record the direct signal from the satellite for the synchronization procedure (Heterodyne Channel HC), while a second high-gain antenna is pointed toward the observed area collecting the signal reflections for imaging (Radar Channel RC). The target area was Metchley Park, located to West (Fig. 6). Table I reports the parameters of two 5 mins long acquisitions exploiting GLONASS P-code transmitted by two different satellites.

TABLE 1. Acquisition Parameters

#	Satellite	Azimuth*	Elevation	PSF orientation*	Resolution cell area
1	732	98°	53°	38°	153 m^2
2	736	75°	75°	-10°	84 m^2

* clockwise from North direction

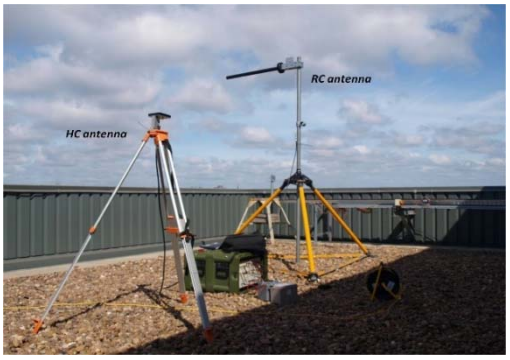

Figure 5. Receiving hardware.

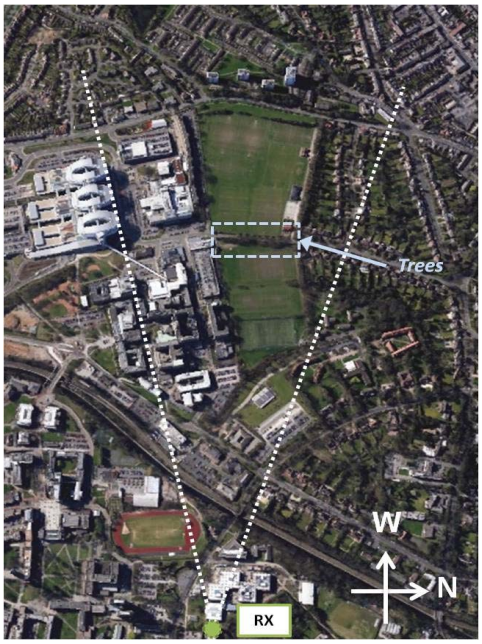

Figure 6. Metchley Park.

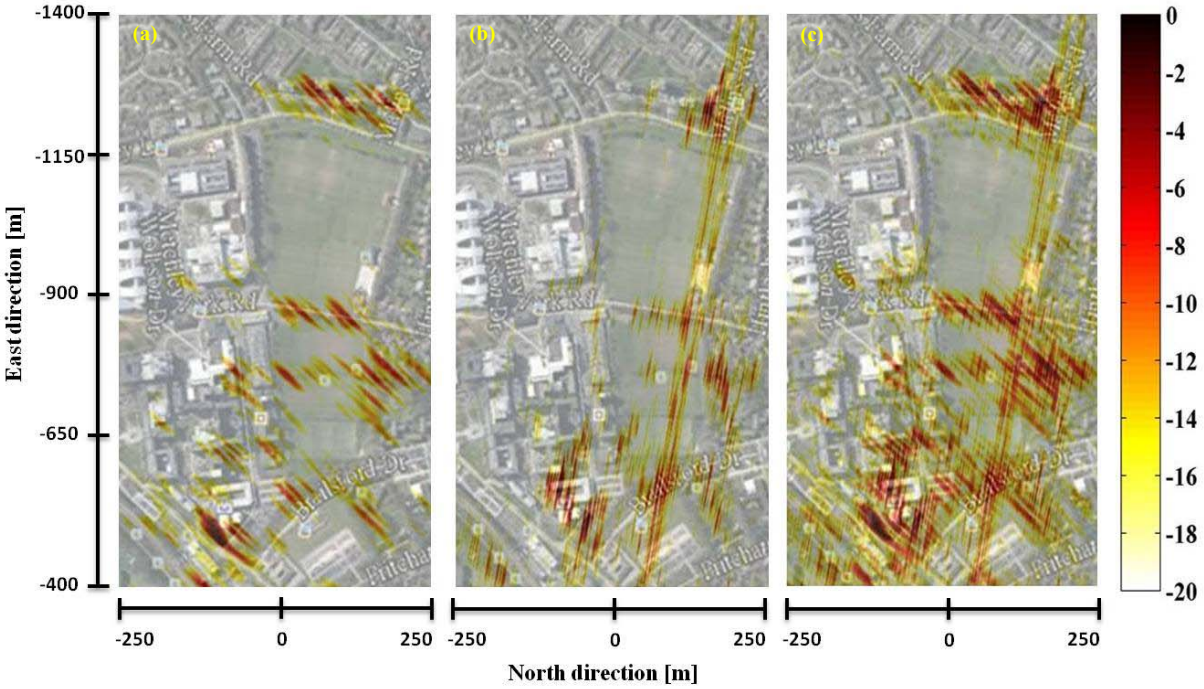

Figure 7. Experimental bistatic (a)-(b) and multistatic (c) images.

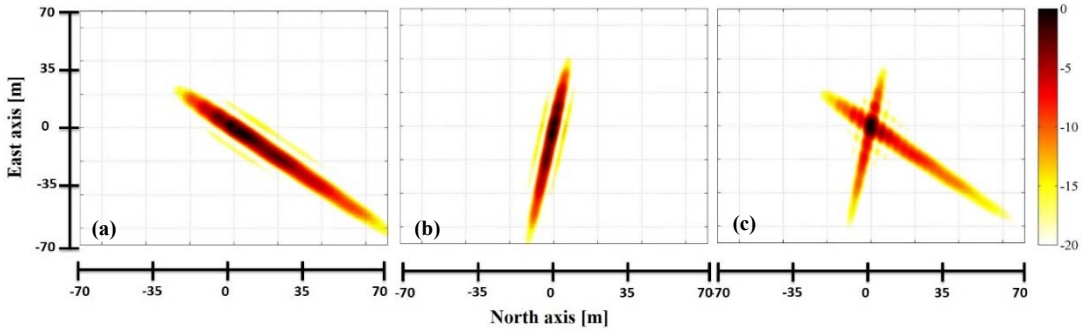

Figure 8. Experimental bistatic (a)-(b) and multistatic (c) point spread functions.

The BSAR and MSAR images are shown in Fig. 7, while Fig. 8 shows the corresponding experimental PSFs obtained by using the direct signal collected by the HC (i.e. the low-gain antenna is acting as a point-like target). By analyzing the bistatic PSFs, one can observe that very large bistatic resolution cells have been obtained (see Table I), which correspond to poor capability in sensing detailed features of the images. However, consequently the different bistatic topologies, resolution ellipses are characterized by a different orientation, being about 48°. This makes possible to form a multistatic image whose experimental PSF (Fig. 8c) has an area of 39 m^2. Looking at the MSAR image in Fig. 7c, we can observe a large number of intersections among the bright spots pertaining to the individual images, providing a deeper level of knowledge about the scene structure. Nevertheless, in many cases, bistatic responses corresponding to different scattering centers intersect in the MSAR image, giving rise to spots of high intensity that do not correspond to any scatterer in the scene and corrupt the quality of the image.

In order to extract the useful information in terms of scattering centers, the joint bi/multi-static CLEAN has been applied against the bistatic and multistatic images (in the case of a bistatic image, the scheme in Fig. 2 is applied for two corresponding BSAR images). For the analysis, we focus on the tree lines at the middle range (Fig. 9). This choice is motivated by the fact that, due to long dwell time and L-band transmission, trees can be considered as a sort of cylindrical scatterers, and an acceptable degree of stability of their scattering centers is expected between the two different perspectives.

Fig. 10a and Fig. 10b show the results obtained from the processing of the two BSAR images. Figures on the top are the radar images superimposed to the optical view of the area. A number of spots can be seen in the patch corresponding the tree lines, and the CLEAN applied against the bistatic images shows some capabilities to extract the scattering centers. Nevertheless, as analyzed in Fig. 3, the poor resolution and the close position of the individual trees entail poor accuracy of single tree identification and consequently scatterer location, as it is

Figure 9. Tree lines.

apparent from the bottom figures showing the comparison among extracted scatterers and actual tree locations.

Results achieved from the multistatic image are shown in Fig. 10c. In this case, the enhanced spatial resolution along with the advanced CLEAN technique allowed identifying with better accuracy the individual trees, so that both the tree lines running along the road have been identified. It is also important to notice that a number of false targets appeared in the radar image (for example the cluster of spots around 100m N, -880m E). Nevertheless, as analyzed in Fig. 4, the algorithm does not recognize them as real scattering centers, so proving the inherent de-ghosting capability of the algorithm.

V. Conclusions

The potential of GNSSs to be exploited as opportunity transmitters for passive multistatic SAR has been investigated in this paper. Specifically, based on the consideration that the bistatic SAR images obtained by different, spatially separated satellites provide bistatic images characterized by differently oriented elliptical image responses, a multistatic image with enhanced resolution can be obtained, able to sense more detailed feature of the observed area. An ad-hoc CLEAN technique is therefore been developed to extract the scattering centers from the images. Such a technique exploits both the bistatic and multistatic images to retrieve the position and complex amplitudes of the dominant scattering centers of the images, and it has an inherent capability to reject the false target positions arising from the multistatic image formation process. Experimental analysis against both point-like scatterers and full images proved the effectiveness of the proposed technique.

References

[1] M. Cherniakov and T. Zeng, "Passive bistatic SAR with GNSS transmitters", in *Bistatic Radar: Emerging Technology*, M. Cherniakov, Ed. New York, NY, USA: Wiley, 2008.

[2] A. Moccia and A. Renga, "Spatial resolution of bistatic synthetic aperture radar: Impact of acquisition geometry on imaging performance," IEEE Trans. on Geosci. and Remote Sens., vol. 49, no. 10, pp. 3487-3503, Oct. 2011.

[3] H. Ma, M. Antoniou, M. Cherniakov, "Passive GNSS-based SAR resolution improvement using joint Galileo E5 signals," IEEE Geosci. Remote Sens. Letters, vol. 12, no. 8, pp. 1640-1644, Aug. 2015

[4] T. Derham, S. Doughty, C. Baker, K. Woodbridge, "Ambiguity Functions for Spatially Coherent and Incoherent Multistatic Radar," IEEE Trans. Aerosp. Electron. Syst., vol 46, no. 1, pp. 230-245, Jan. 2010.

[5] T. Lindgren, D. M. Akos, "A Multistatic GNSS Synthetic Aperture Radar for Surface Characterization," IEEE Trans. on Geosci. and Remote Sens., vol. 46, no. 8, pp.2249-2253, Aug. 2008.

[6] F. Santi, M. Antoniou, D. Pastina, "Point Spread Function Analysis for GNSS-Based Multistatic SAR," IEEE Geosci. Remote Sens. Letters, vol. 12, no. 2, pp. 304-308, Feb. 2015.

[7] F. Santi, M. Bucciarelli, D. Pastina, M. Antoniou, D. Tzagkas, M. Cherniakov, "Passive multistatic SAR with GNSS transmitters: preliminary experimental results," Proc. of EuRAD 2014, Oct. 2014.

[8] T. Zeng *et al*., "Multiangle BSAR Imaging Based on BeiDou-2 navigation Satellite System: Experiments and Preliminary Results," IEEE Trans. on Geosci. and Remote Sens., vol. 53, no. 10, p. 5760-5773, Oct. 2015.

[9] F. Santi, M. Bucciarelli, D. Pastina, M. Antoniou, "CLEAN technique for passive bistatic and multistatic SAR with GNSS transmitters," Proc. 2015 IEEE Radar Conference, pp.1228-1233, May 2015.

[10] M. Antoniou, M. Cherniakov, "GNSS-based SAR: A signal processing view," EURASIP J. Adv. Signal Process., 2013:98, May 2013.

[11] T. Zeng, M. Cherniakov, and T. Long, "Generalized Approach to Resolution Analysis in BSAR," IEEE Trans. Aerosp. Electron. Syst., vol. 41, no. 2, pp.461-471, Apr. 2005.

[12] J. Tsao and B. D. Steinberg, "Reduction of sidelobes and speckle artifacts: The CLEAN technique," IEEE Trans. Antennas Propag., vol. 36, no. 4, pp. 543-556, Apr. 1988.

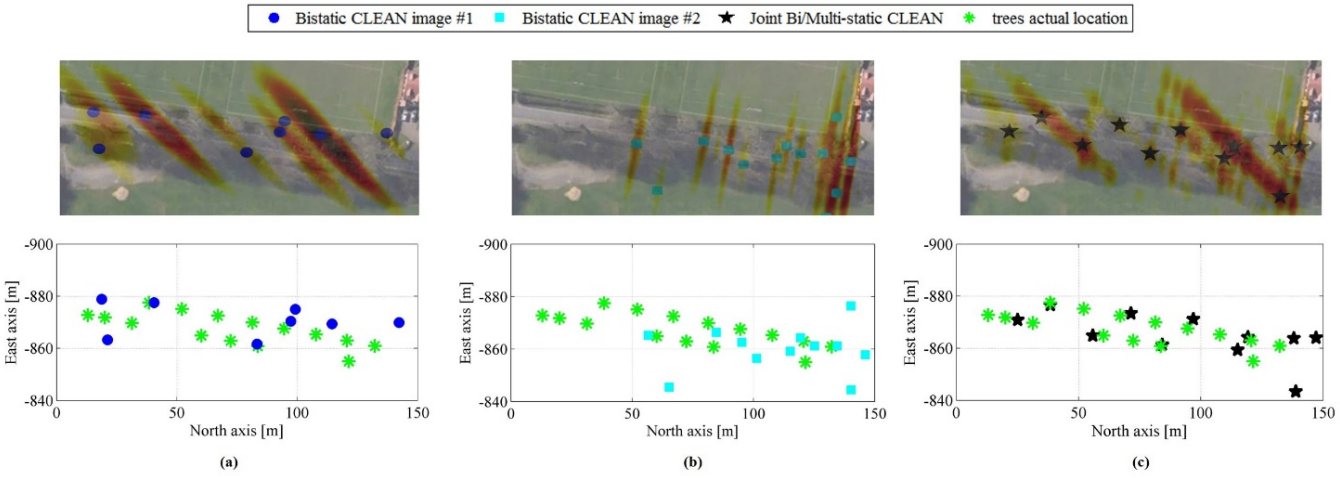

Figure 10. Tree lines area results for BSAR #1 (a), #2 (b) and MSAR (c) images.